Heliyon 10 (2024) e40257

Contents lists available at ScienceDirect

Heliyon

journal homepage: www.cell.com/heliyon

Research article

The heat transfer in skin tissues under the general two-temperature three-phase-lag model of heat conduction with a comparative study

Eman A.N. Al-Lehaibi [a], Hamdy M. Youssef [b,*]

[a] Mathematics Department, Jamoum University College, Umm Al-Qura University, Jamoum, Saudi Arabia
[b] Mechanical Engineering Department, College of Engineering and Architecture, Umm Al-Qura University, Makkah, 21955, Saudi Arabia

ARTICLE INFO

Keywords:
Three-phase-lag
Skin tissue
Dual-phase-lag
Two-temperature
Ramp-type heat
Thermomass motion
Drift velocity

ABSTRACT

In this paper, a new and more general model of heat conduction that depends on the drift velocity due to thermomass motion assumption will be established and will be applied to the skin tissue. Four different heat conduction models will be incorporated into a unified equation of heat conduction: the Pennes, Vernotte-Cattaneo, dual-phase-lag of Tzou, and the general two-temperature three-phase-lag of Youssef. The governing partial differential equations of the general two-temperature three-phase-lag model of bioheat conduction will be implemented and solved directly in the domain of the Laplace transformation. The numerical solutions of the Laplace transform will be calculated by executing the Tzou iteration formula. The ramp-type heat on the surface of the skin tissue will be considered as thermal loading. The conductive and dynamic temperature increment reactions have been studied and discussed with different values of ramp-time heat, characteristic length, and drift velocity parameters. The novelty of this work is to introduce some comparisons of the four under-studied bioheat conduction models and show the differences between them in the figures. The numerical results show that the ramp-time heat, drift velocity, and characteristic length parameters have major impacts on the increment of both dynamical and conductive temperature distributions.

1. Introduction

The transfer of heat via live skin tissue has a fundamental role in the administration of many medications. With the microwave's aid, lasers, and other novel technologies, the field of bioheat transfer has expanded as well [1]. Pennes describes the methodology used in biothermal transmission experiments in genuine biological tissues. Pennes derived the first bioheat transfer and enhanced the parabolic type of the model to be suitable for biological tissues [2]. Pennes's technique is applied to simulate the behaviour and regularity of temperature fluctuations in biological tissues and living organisms. The observed patterns do not exhibit either Fourier or hyperbolic behaviour. To describe this kind of hyperbolic equation, Cattaneo and Vernotte introduced slight adjustments to Fourier's heat transfer rule in its first-order linear expansion form [3,4]. To assess the impact of thermal flux action and microwaves, a thermal wave model was devised. A multitude of methods have been devised to treat different types of skin tissues while ensuring the safety of the surrounding healthy tissue. The dual-phase-lag (DPL), hyperbolic, and parabolic bioheat transport models have been used to

* Corresponding author.
E-mail addresses: ealehaibi@uqu.edu.sa (E.A.N. Al-Lehaibi), youssefanne2005@gmail.com, hmyoussef@uqu.edu.sa (H.M. Youssef).

https://doi.org/10.1016/j.heliyon.2024.e40257
Received 19 July 2024; Received in revised form 10 October 2024; Accepted 7 November 2024
Available online 8 November 2024

investigate the non-Fourier thermomechanical behaviour of skin tissues under various surface thermal loading constraints. Xu and his colleagues observed notable differences among Pennes's model, thermal wave model, and dual-phase-lag (DPL) anticipations model [5]. In their study, Rossmann et al. studied the relationship between temperature and the effects on blood perfusion, thermal properties, and dielectric characteristics of biological tissues at ablation and hyperthermic temperatures [6]. The dual-phase-lag (DPL) approach has been applied to explore Tzou's model by including the time-delayed activity at a rapid rate of response. The prompt identification of the small-scale reaction is expedited, despite the method's time-consuming nature [7,8]. Tzou established the phase lag for a temperature gradient [9]. Askarizadeh et al. used the dual-phase-lag (DPL) bioheat conduction model to address the challenges associated with heat transmission through the skin tissues [10]. Dutta and Kundu developed a thermal model of two-dimensional tumour tissues to get a deeper understanding of the two-dimensional local thermal unbalanced treatment model [11].

The hyperthermia process is employed to assess the model of two-stage for heat transfer issues in living tissue [12–14], whereas Liu and Chen's heat conduction model utilizes non-Fourier thermal interactions to characterize the thermal transit through the biological tissues to determine hyperthermia [15]. Zhang enhanced the phase lag, known as relaxation times, by considering the effect of the properties of the blood and skin tissue, the rate of perfusion, and the interphase charge of the heat transfer parameter [16]. He observed the lap times for live tissues are quite similar. Dutta and Kundu introduced a study on the transmission of thermal waves to detect hyperthermia in biological tissue. They examined how heat flows continuously and variably across the surface of the skin tissue [17]. Poor et al. used the dual-phase-lag (DPL) bioheat transfer model to examine the skin tissue as a finite domain for cosine, continuous, and pulse flow of heat conditions on the bounding surface of the skin tissue [18]. Liu and Xu constructed a novel analytical approach of closed form to solve Pennes's model for changes in living skin tissue temperature caused by heat flow of sinusoidal type [19]. Ahmadika et al. derived an analytical solution of the hyperbolized bioheat transfer model and the parabolized bioheat model of Pennes's equations under periodic constant and pulsed heat flow boundary conditions [20]. Youssef and Alghamdi have examined the use of a one-dimensional thermoelastic dual-phase-lag model to study the behaviour of skin tissue under heat stress [21]. Youssef and El-Bary examined the thermal harm inflicted on various cancer tissues due to the thermoelectrical influence, specifically focusing on the Thomson effect. This study examined and evaluated the specific electrical properties of three different kinds of cancer tissues [22].

Youssef and Salem studied the temperature interaction and response of skin tissues under continuous heat flow caused by thermoelectrical shock on the skin tissue's boundary. They used the bioheat conduction equation based on the dual-phase-lag (DPL) and Tzou models for their investigation [23]. The thermomass theory is used to examine non-Fourier heat conduction. Heat flux refers to the controlled transfer of thermal energy over a temperature gradient, where thermal energy is carried by the relativistic mass associated with heat conduction. The thermomass motion equation has been derived by building upon Newtonian mechanics as the basis for the heat conduction equation. The non-Fourier heat conduction phenomenon may be attributed to the significant inertia effect caused by thermomass motion. This hypothesis, together with the consideration of drift velocity, explains non-Fourier heat conduction. Thermomass theory has predicted the occurrence of non-Fourier heat conduction in a stable state [24]. Youssef developed an original and distinctive theory of two-temperature generalized thermoelasticity, which is based on the concept of thermomass motion [25]. Youssef and Al-Lehaibi introduced a new theory and new model of generalized thermoelasticity based on thermomass gas flow with low drift velocity and linear resistance, within the framework of the non-Fourier law of heat conduction with first-order expansion and one relaxation time. The heat conduction equation, derived from the total derivative of the thermomass gas velocity, now incorporates the resistance effect [26]. May discuss how understanding heat transfer in skin tissues is crucial for improving medical treatments such as laser therapy, which relies on precise temperature control to avoid damage to surrounding tissues [27–35].

This study will establish a new gene heat transfer model that takes thermomass motion into account and examines it on skin tissue. A unified equation for heat transmission has been made to include four different models: the Pennes, Vernotte-Cattaneo, Tzou (DPL), and Youssef (GTTTPL) models where the authors of the current work hope to introduce a new and successful heat conduction model in which the thermal wave behaviour is closer to the real behaviour than the other mention models. The equations that control the general two-temperature three-phase-lag (GTTTPL) bioheat transmission model have been put into the Laplace transform domain and solved directly there. Using Tzou iteration, the numerical inversions and numerical solutions of the Laplace transforms have been found. The ramp-type heat on the skin's surface has been thought about. We got and talked about the temperature increase responses when the ramp-time heat parameter, characteristic length, and drift velocity parameters were changed. The results also show a comparison of the four bioheat transmission models that are under study.

2. The basic steps of the current work

2.1. The two-temperature classical Fourier law of bioheat transfer (Youssef-Pennes's model)

Pennes' model of biological skin tissues is derived from the classical Fourier's law of heat conduction as follows [21,32–37]:

$$q_{i,i} = -\rho C\dot{\theta} - \rho_b C_b w_b \theta + Q \tag{1}$$

The classical Fourier law of heat conduction is in the well-known following form [2]:

$$q_i = -K\varphi_{,i} \tag{2}$$

The two-temperature equation is as follows [25,37,37]:

$$\boldsymbol{\varphi} - \theta = a\varphi_{,ii} \tag{3}$$

Then, we have two-temperature Penne's heat conduction law as follows [1–7]:

$$\boldsymbol{K}\varphi_{,ii} = \rho C\dot{\theta} + \rho_b C_b w_b \theta - Q, \tag{4}$$

where $\boldsymbol{K}, C$ and $\boldsymbol{\rho}$ are the thermal conductivity, specific heat, and density, respectively, of the skin tissue. Moreover, $\boldsymbol{\theta} = T_D - T_b, \varphi = T_C - T_b$ gives the dynamical temperature increment and conductive temperature increment, respectively, where T_D, T_C and T_b are the absolute dynamic temperature, absolute conductive temperature, and blood temperature, respectively, while $\boldsymbol{a} \geq 0$ is called the two-temperature parameter, moreover $\boldsymbol{a} = 0$ gives the one-temperature model. In addition, C_b, w_b, ρ_b and T_b give the specific heat of the blood, blood perfusion rate, blood density, and blood temperature, respectively. $\boldsymbol{Q} = Q_{met} + Q_{ext}$ where Q_{met} gives the metabolic heat due to the biochemical interaction through the skin tissue. Q_{ext} gives the external heat source.

2.2. The two-temperature non-Fourier law of bioheat transfer (Youssef-Vernotte-Cattaneo's model)

Vernotte-Cattaneo (V-C) modified the classical Fourier thermal conduction law by including a limited speed of thermal wave propagation and considering the latency time of the heat flow in the non-Fourier law of heat conduction [3–8,21,32–37]:

$$-K\varphi_{,i} = q_i|_{t\to t+\tau_q} = q_i + \tau_q \dot{q}_i \tag{5}$$

Therefore, we have the hyperbolic form of the heat conduction law of Vernotte-Cattaneo (V-C) as follows [21,32–37]:

$$\boldsymbol{K}\,\varphi_{,ii} = \left(1 + \tau_q \frac{\partial}{\partial t}\right)(\rho C\dot{\theta} + w_b C_b \rho_b \theta - Q) \tag{6}$$

where $\tau_q = \frac{\alpha}{c_0^2} \geq 0$ (for hyperbolic heat conduction equation) is one of the material properties which is called the heat flux lag-time of relaxation time parameter of the heat flux, where $\tau_q = 0$ gives the parabola heat conduction equation. Moreover, α gives the thermal diffusivity, while c_0 denoting the propagation speed of the thermal wave inside the material.

2.3. The two-temperature dual-phase-lag (TTDPL) model of bioheat transfer (Youssef-Tzou's model)

To derive Tzou's model, the dual-phase-lag (DPL) model in which the bioheat conduction equations depend on the dual reaction between the heat flux q_i and the gradient of the temperature $T_{,i}$, have been re-modified by Tzou to be in the following form [21,32–37]:

$$q_i|_{t\to t+\tau_q} = -K\varphi_{,i}|_{t\to t+\tau_C} \tag{7}$$

which gives after using Maclurin's expansion up to the first-order derivative [21,32–37]:

$$\left(1 + \tau_q \frac{\partial}{\partial t}\right) q_i = -K\left(1 + \tau_C \frac{\partial}{\partial t}\right)\varphi_{,i} \tag{8}$$

Thus, Tzou's bioheat conduction model takes the following two differential equations [21,32,34]:

$$\boldsymbol{K}\left(1 + \tau_C \frac{\partial}{\partial t}\right)\varphi_{,ii} = \left(1 + \tau_q \frac{\partial}{\partial t}\right)(\rho C\dot{\theta} + w_b C_b \rho_b \theta - Q) \tag{9}$$

and

$$\boldsymbol{\varphi} - \theta = a\left(1 + \tau_C \frac{\partial}{\partial t}\right)\varphi_{,ii} \tag{10}$$

where $\tau_C \geq 0$ is called the second lag time or the second relaxation time parameter due to the phase lag of the conductive temperature gradient passing through the material.

2.4. The general two-temperature three-phase-lag (GTTTDPL) model of bioheat Trnafer (Youssef's model)

The thermomass motion equation is obtained by the application of Newtonian mechanics, and it serves as the fundamental equation for heat conduction. The substantial influence of thermomass inertia enhances our comprehension of non-Fourier heat conduction resulting from the thermomass theory. The Thermomass consideration suggests that non-Fourier heat conduction may occur in a thermally stable environment. In the setting of a low-speed thermomass gas flow, Moran Wang et al. developed a comprehensive heat conduction model that applies to a continuous medium [26].

$$-K(1-\beta)\varphi_{,i} = \left(1 + \tau_q \frac{\partial}{\partial t}\right) q_i - \rho C \ell_i \dot{\theta} + \ell_i \left(1 + \tau_q \frac{\partial}{\partial t}\right) q_{j,j} \tag{11}$$

where $\tau_q = \frac{K}{2\alpha\rho C^2 \widetilde{T}}$ is the heat flux q lag-time parameter, $\ell_i = \frac{K\,\widetilde{q}_i}{2\alpha C(\rho C\widetilde{T})^2}$ is the characteristic length, $\beta = \frac{\widetilde{q}^2}{2\alpha\rho^2 C^3 \widetilde{T}^3}$ is a non-dimensional

parameter which characterizes the compressibility of the phonon gas flow, while $\widetilde{T}$ and $\widetilde{q}$ are the points of the equilibrium states for absolute temperature and heat flux, respectively.

Considering $\tau_C \geq 0$ and $\tau_D \geq 0$ are the lag-time parameters of the conductive and dynamic temperature increment's gradient $\theta_{,i}$ and $\varphi_{,i}$, then, we have [25,36,37]:

$$\varphi_{,i}\big|_{t\to t+\tau_C} = \left(1+\tau_C\frac{\partial}{\partial t}\right)\varphi_{,i} \tag{12}$$

and

$$\theta_{,i}\big|_{t\to t+\tau_D} = \left(1+\tau_D\frac{\partial}{\partial t}\right)\theta_{,i} \tag{13}$$

Thus, equation (11) takes the following form [26]:

$$-K(1-\beta)\left(1+\tau_C\frac{\partial}{\partial t}\right)\varphi_{,i} = \left(1+\tau_q\frac{\partial}{\partial t}\right)q_i - \rho C\ell_i\,\dot{\theta} + \ell_i\left(1+\tau_q\frac{\partial}{\partial t}\right)q_{j,j} \tag{14}$$

The above equation gives the following equation [26]:

$$-K(1-\beta)\left(1+\tau_C\frac{\partial}{\partial t}\right)\varphi_{,ii} = \left(1+\tau_q\frac{\partial}{\partial t}\right)q_{i,i} - \rho C\ell_i\,\dot{\theta}_{,i} + \ell_i\left(1+\tau_q\frac{\partial}{\partial t}\right)q_{j,ij} \tag{15}$$

By using equation (12) again, we obtain [26]:

$$\boldsymbol{K}(1-\beta)\left(1+\tau_C\frac{\partial}{\partial t}\right)\varphi_{,ii} = \rho C\ell_i\left(1+\tau_D\frac{\partial}{\partial t}\right)\dot{\theta}_{,i} - \left(1+\tau_q\frac{\partial}{\partial t}\right)q_{i,i} - \ell_i\left(1+\tau_q\frac{\partial}{\partial t}\right)q_{j,ij} \tag{16}$$

From equation (1) and equation (16), we obtain the general heat conduction equation including three-phase-lag parameters in the form [26]:

$$\begin{aligned}(1-\beta)K\left(1+\tau_C\frac{\partial}{\partial t}\right)\varphi_{,ii} &= \rho C\ell_i\left(1+\tau_D\frac{\partial}{\partial t}\right)\left(2+\tau_q\frac{\partial}{\partial t}\right)\dot{\theta}_{,i} + \rho C\left(1+\tau_q\frac{\partial}{\partial t}\right)\dot{\theta}\\ &+\rho_b C_b w_b\left(1+\tau_q\frac{\partial}{\partial t}\right)\left[\theta+\left(1+\tau_D\frac{\partial}{\partial t}\right)\ell_i\theta_{,i}\right] - \left(1+\tau_q\frac{\partial}{\partial t}\right)(Q+\ell_i Q_{,i})\end{aligned} \tag{17}$$

and

$$\boldsymbol{\theta} = \varphi - a\left(1+\tau_C\frac{\partial}{\partial t}\right)\varphi_{,ii} \tag{18}$$

The above system of coupled two differential equations gives the model of general two-temperature three-phase-lag (GTTTDPL) heat conduction in the context of the thermomass motion and it generates four different heat conduction models when $\boldsymbol{\beta} \neq 0, \ell_i \neq 0$, and $a \neq 0$ as follows:

1. The parameters $\tau_q = \tau_D = \tau_C = 0$ give the classical two-temperature Fourier law of bioheat transfer (Pennes-2Temp.) based on two temperature considerations.
2. The parameters $\tau_q \neq 0, \tau_D = \tau_C = 0$ give the two-temperature non-Fourier law of bioheat transfer (Vernotte-Cattaneo-2Temp.) based on two-temperature consideration.
3. The parameters $\tau_q \neq 0, \tau_D = \tau_C \neq 0$ give the two-temperature dual-phase-Lag (TTDPL) of bioheat transfer (Tzou-2Temp.) based on two-temperature consideration.
4. The parameters $\tau_q \neq 0, \tau_D \neq 0, \tau_C \neq 0$ give the general two-temperature three-phase-Lag (GTTTPL) of bioheat transfer (Youssef-2Temp.).

Hence, the one-dimensional heat conduction equations (GTTTPL) take the following forms [25,26]:

$$\begin{aligned}(1-\beta)\left(1+\tau_C\frac{\partial}{\partial t}\right)\frac{\partial^2\varphi}{\partial x^2} &= \eta\ell\left(1+\tau_D\frac{\partial}{\partial t}\right)\left(2+\tau_q\frac{\partial}{\partial t}\right)\frac{\partial\dot{\theta}}{\partial x} + \eta\left(1+\tau_q\frac{\partial}{\partial t}\right)\dot{\theta}\\ &+\eta_b\left(1+\tau_q\frac{\partial}{\partial t}\right)\left[\theta+\left(1+\tau_D\frac{\partial}{\partial t}\right)\ell\frac{\partial\theta}{\partial x}\right] - \frac{Q_{met}}{K}\end{aligned} \tag{19}$$

and

$$\boldsymbol{\theta} = \varphi - a\left(1+\tau_C\frac{\partial}{\partial t}\right)\frac{\partial^2\varphi}{\partial x^2} \tag{20}$$

where $=\frac{\rho C}{K}, \eta_b = \frac{\rho_b C_b w_b}{K}$.

We consider the skin tissue to be at rest initially, then, we have the upcoming initial conditions [23–26]:

$$\boldsymbol{\theta}(x,0) = \left.\frac{\partial \theta(x,t)}{\partial t}\right|_{t=0} = 0 \tag{21}$$

and

$$\boldsymbol{\varphi}(x,0) = \left.\frac{\partial \varphi(x,t)}{\partial t}\right|_{t=0} = 0 \tag{22}$$

The Laplace transforms will be applied as follows [23–26]:

$$\boldsymbol{L}\{f(x;t)\} = \int_0^{\infty} f(x;t)e^{-s\,t}\,dt = F(x;s), 0 \le t < \infty \text{and } s > 0 \tag{23}$$

and the inversions of the Laplace transforms could be obtained by applying the following iteration form [38]:

$$L^{-1}\{\bar{f}(x;s)\} = f(x;t) \approx \mathrm{Re}\left\{\frac{e^{\kappa t}}{t}\left[\frac{1}{2}F(x;\kappa) + \sum_{j=1}^{J}(-1)^j F\left(x;\kappa + \frac{i\,j\,\pi}{t}\right)\right]\right\} \tag{24}$$

where $\boldsymbol{i} = \sqrt{-1}$ is the imaginary number unit, "Re" denotes the real part of a complex function, and $\boldsymbol{J}$ is an integer parameter that could be chosen such that [38]:

$$|f(x,t)_{J+1} - f(x,t)_J| \ll 10^{-10} \tag{25}$$

To obtain a faster convergence for the above iteration, some experiments verified that the parameter " $\boldsymbol{\kappa}$"may satisfy the following relation $\boldsymbol{\kappa} \approx \frac{4.7}{t}$ [7,38].

Hence, we obtain:

$$\frac{d^2\overline{\varphi}}{dx^2} = \alpha_1\frac{d\overline{\theta}}{dx} + \alpha_2\overline{\theta} - \psi_1 \tag{26}$$

and

$$\overline{\theta} = \overline{\varphi} - \alpha_3\frac{d^2\overline{\varphi}}{dx^2} \tag{27}$$

where

$$\alpha_1 = \frac{\ell(1+\tau_D s)\left[\eta\left(2+\tau_q s\right)s + \eta_b\left(1+\tau_q s\right)\right]}{(1-\beta)(1+\tau_C s)}, \alpha_2 = \frac{\left(1+\tau_q s\right)(\eta s + \eta_b)}{(1-\beta)(1+\tau_C s)}, \alpha_3 = a(1+\tau_C s),$$

$$\psi_1 = \frac{Q_{met}}{s(1-\beta)(1+\tau_C s)K}$$

By eliminating $\overline{\theta}$, we get the following ordinary linear differential equation with third order:

$$\frac{d^3\overline{\varphi}}{dx^3} + L\frac{d^2\overline{\varphi}}{dx^2} - M\frac{d\overline{\varphi}}{dx} - N\overline{\varphi} = -\psi_2 \tag{28}$$

where $L = \frac{(1+\alpha_2\alpha_3)}{\alpha_1\alpha_3}, M = \frac{1}{\alpha_3}, N = \frac{\alpha_2}{\alpha_1\alpha_3}, \psi_2 = \frac{\psi_1}{\alpha_1\alpha_3}$.

The general solution of the differential equation (28) takes the following form:

$$\overline{\varphi}(x,s) = \varphi_1(s)e^{\lambda_1 x} + \varphi_2(s)e^{\lambda_2 x} + \varphi_3(s)e^{\lambda_3 x} + \frac{\psi_2}{N} \tag{29}$$

where $\lambda_1, \lambda_2,$ and λ_3 are the complex roots of the following auxiliary equation (characteristic equation):

$$\lambda^3 + L\lambda^2 - M\lambda - N = 0 \tag{30}$$

and $\varphi_1(s), \varphi_2(s),$ and $\varphi_3(s)$ are some parameters to be determined by applying any set of boundary conditions.

The dynamic temperature increment function $\overline{\theta}(x,s)$ takes the following form:

$$\overline{\theta}(x,s) = \left(1-\alpha_3\lambda_1^2\right)\varphi_1(s)e^{\lambda_1 x} + \left(1-\alpha_3\lambda_2^2\right)\varphi_2(s)e^{\lambda_2 x} + \left(1-\alpha_3\lambda_3^2\right)\varphi_3(s)e^{\lambda_3 x} + \frac{\psi_2}{N} \tag{31}$$

Now, assuming the skin tissue occupies the one-dimensional region $0 \le x \le h$, and obeys the differential equation in (28) as in Fig. 1:

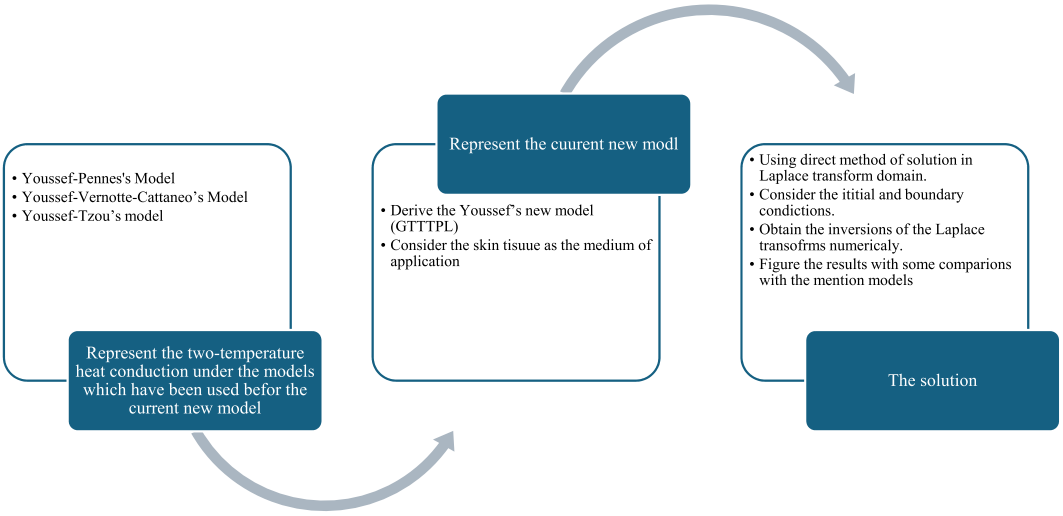

Fig. 1. The flowchart of the work.

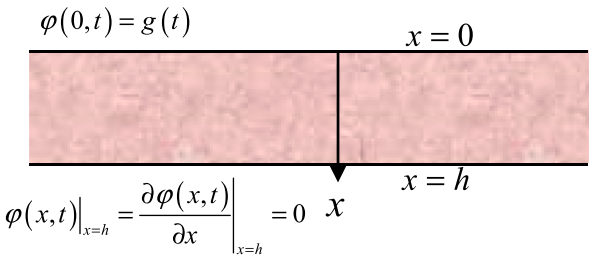

Fig. 2. The material of the skin tissue occupies the one-dimensional region $0 \le x \le h$.

We consider that the bounding plane of the outer surface is thermally loaded with a time function $g(t)$ which is ramp-type heat, while the inner surface has neither conductive temperature increment nor heat flux as in Fig. 2.

The boundary conditions are [25,26]:

$$\varphi(x,t)|_{x=0}=g(t)=\left\{\begin{array}{ll}\dfrac{t}{t_0} & 0\le t<t_0\\ 1 & t\ge t_0\end{array}\right\} \tag{32}$$

and

$$\varphi(x,t)|_{x=h}=\left.\frac{\partial\varphi(x,t)}{\partial x}\right|_{x=h}=0 \tag{33}$$

After applying the Laplace transform on the above boundary conditions, we obtain that [25,26]:

$$\overline{\varphi}(0,s)=G(s)=\frac{1-e^{-st_0}}{s^2t_0} \tag{34}$$

and

$$\overline{\varphi}(h,s)=\left.\frac{d\overline{\varphi}(x,s)}{dx}\right|_{x=h}=0 \tag{35}$$

By applying the boundary conditions (34) in the general solution (29), we obtain:

$$\varphi_1(s)+\varphi_2(s)+\varphi_3(s)=G(s)-\frac{\psi_2}{N} \tag{36}$$

$$\varphi_1(s)e^{\lambda_1 h}+\varphi_2(s)e^{\lambda_2 h}+\varphi_3(s)e^{\lambda_3 h}=-\frac{\psi_2}{N} \tag{37}$$

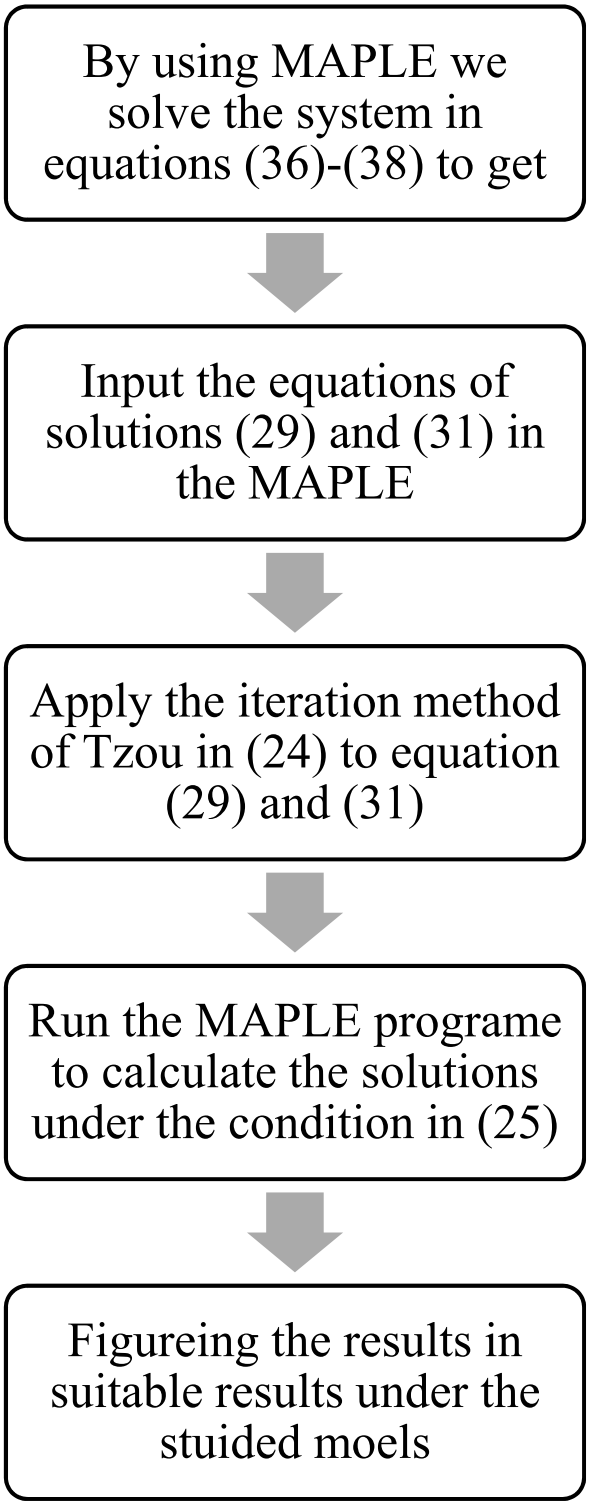

Fig. 3. The flowchart of the numerical calculation using the MAPLE program.

Table 1
The skin tissue and blood's properties [16,21,32–39].

Parameter	Value	Unit	Parameter	Value	Unit
$\boldsymbol{\rho}$	1000	kg/m^3	T_b	37	°C
ρ_b	1060	kg/m^3	τ_T, τ_q	30.0, 10.0	s
$\boldsymbol{K}$	0.215	**W**/m °C	W_b	0.00052	**ml**/C m
$\boldsymbol{C}$	4187	**J**/kg °C	t_0	100.0	s
C_b	3800	**J**/kg °C	h	0.01	m

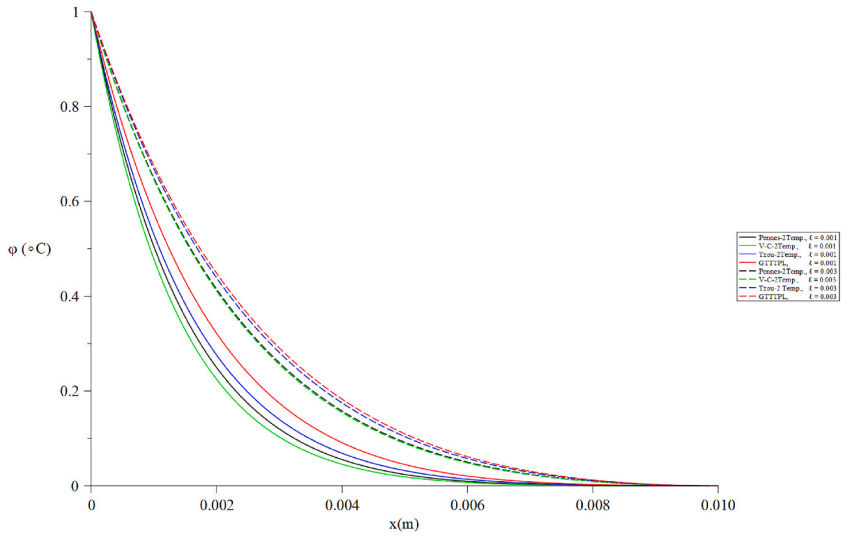

Fig. 4. The distributions of the conductive temperature increment under different models and variance characteristic length values $\ell = \{0.001, 0.003\}$ when $\neq 0$, and $t = t_0 = 60(s)$.

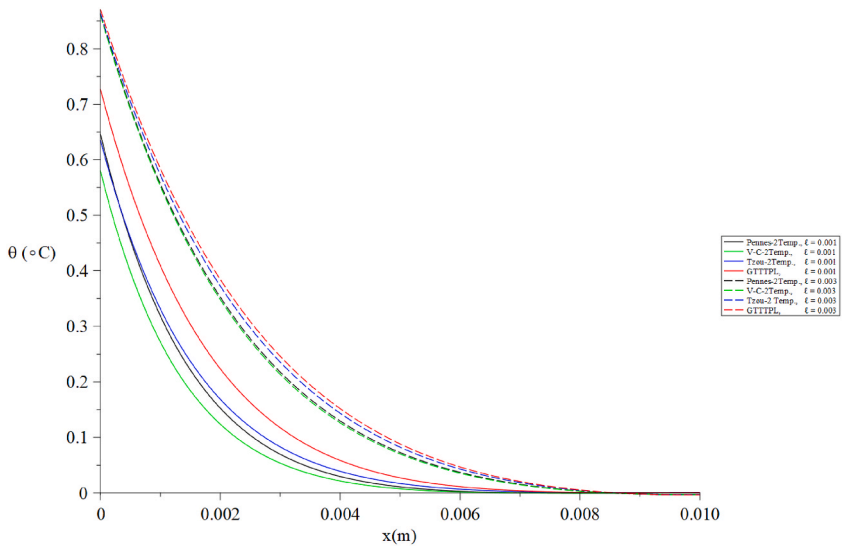

Fig. 5. The distributions of the dynamic temperature increment under different models and variance of characteristic length values $\ell = \{0.001, 0.003\}$ when $\neq 0$, and $t = t_0 = 60(s)$.

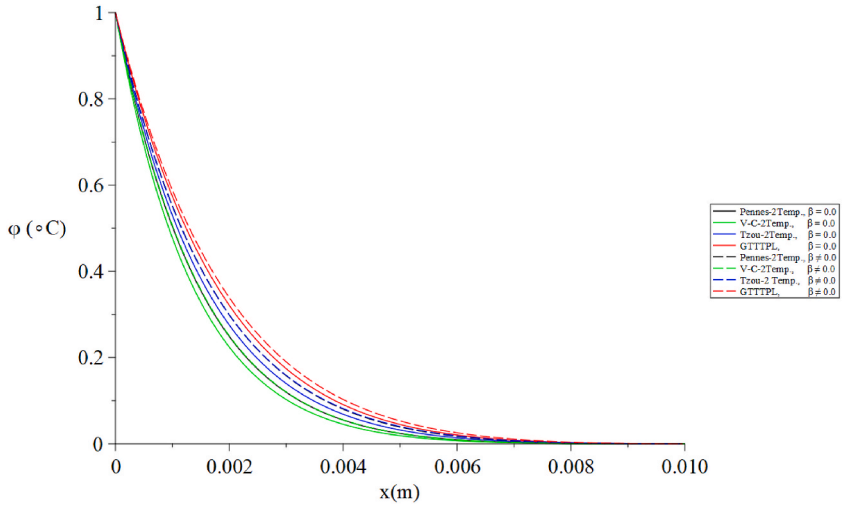

Fig. 6. The distributions of the conductive temperature increment under different models and variance drift velocity values when $\ell = 0.001$ and $t = t_0 = 60(s)$.

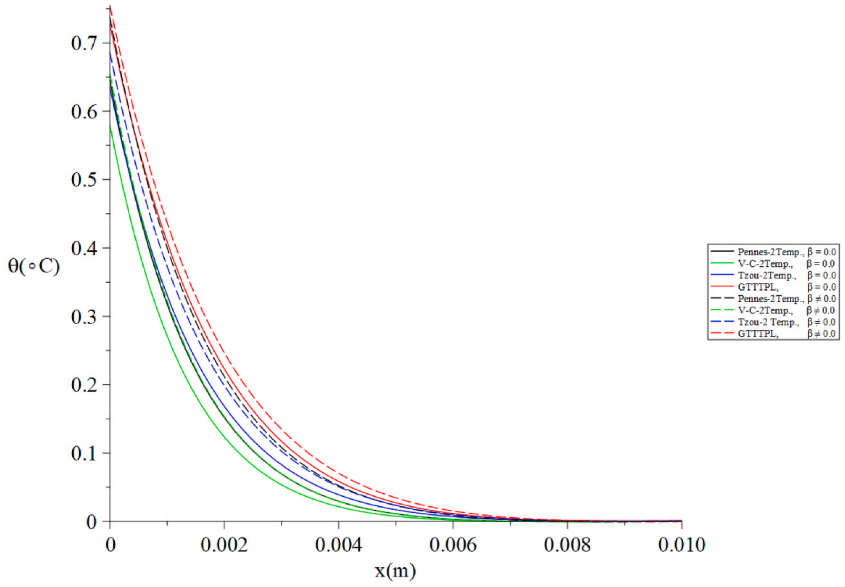

Fig. 7. The distributions of the dynamic temperature increment under different models and variance drift velocity values when $\ell = 0.001$ and $t = t_0 = 60(s)$.

$$\lambda_1^2\varphi_1(s)e^{\lambda_1 h} + \lambda_2^2\varphi_2(s)e^{\lambda_2 h} + \lambda_3^2\varphi_3(s)e^{\lambda_3 h} = 0 \tag{38}$$

After getting the parameters $\varphi_1, \varphi_2, \varphi_3$, the final solution in the original time domain could be calculated by executing computationally the Tzou's iteration (24).

3. Numerical results and discussions

This study examines the two-temperature distributions within skin tissue using four bioheat transfer models which are understudied (Youssef-Pennes, Youssef-Vernotte-Cattaneo, Youssef-Tzou, and GTTTPL of Youssef). The steps to obtain the numerical solution have been shown by the flowshart in Fig. 3.

Table 1 displays the values with units of the thermal parameters of the skin tissue which have been used in the current calculations:

Figs. 4 and 5 illustrate the distributions of the conductive temperature increment and dynamical temperature increment, respectively, based on the four studied models and different characteristic length values $\ell = \{0.001, 0.003\}$ when $t = t_0 = 60(s)$

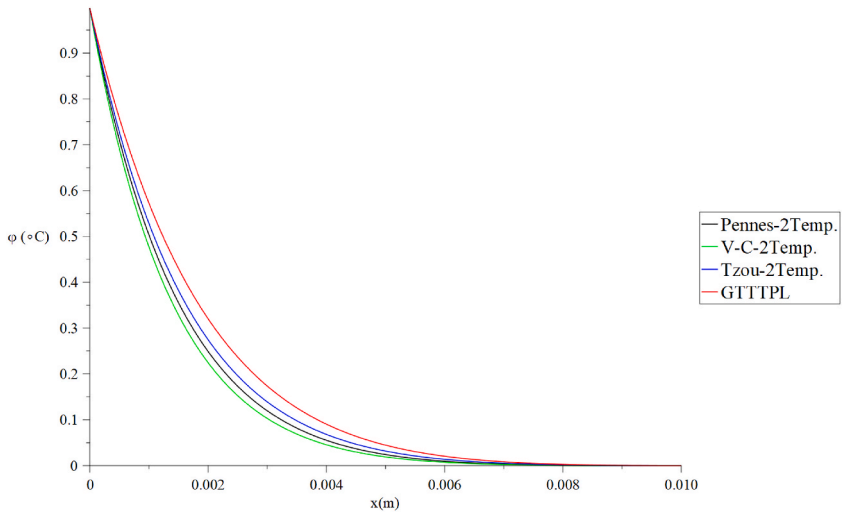

Fig. 8. The distributions of the conductive temperature increment distribution under different models when $\ell = 0.001$, $\beta \neq 0$, and $t(50\,\text{s}) > t_0(45\,\text{s})$.

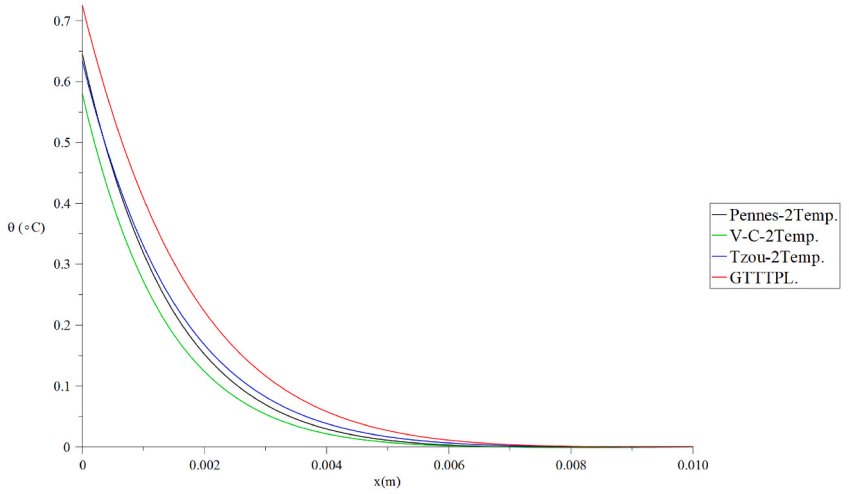

Fig. 9. The distributions of the dynamic temperature increment distribution under different models when $\ell = 0.001$, $\beta \neq 0$, and $t(50\,\text{s}) > t_0(45\,\text{s})$.

standing on the effect of the characteristic length on the thermal interaction on the skin tissue.

Fig. 4 shows that the effect of the characteristic length is significant on the conductive temperature, where increasing its value leads to an increase in the conductive temperature increment. Moreover, decreasing the value of the characteristic length leads to an increase in the difference between the values of the conductive temperature in the context of the four studied models. In other words, increasing the value of characteristic length makes the four studied more closely, especially the Pennes and Vernotte-Cattaneo models. In addition, decreasing the value of characteristic length makes the thermoconductive wave fall to zero quickly under the four studied models. Furthermore, the conductive temperature increases values, as determined by the four models under study, follow the following sequence [1–7,25,26]:

$$\boldsymbol{\varphi}(\text{GTTTPL}) > \varphi(\text{Tzou} - 2\text{temp.}) > \varphi(\text{Pennes} - 2\text{temp.}) > \varphi(\text{V} - \text{C} - 2\text{temp.}) \tag{39}$$

Fig. 5 illustrates the impact of the characteristic length is significant on the conductive temperature because increasing its value leads to an increase in the dynamical temperature increment. Moreover, decreasing the value of the characteristic length leads to an increase in the difference between the values of the dynamical temperature in the context of the four studied models. In other words, increasing the value of characteristic length makes the four studied more closely, especially the Pennes and Vernotte-Cattaneo models. In addition, the values of dynamical temperature increment based on the four studied models take the following order [1–7,25,26]:

$$\boldsymbol{\theta}(\text{GTTTPL}) > \theta(\text{Tzou} - 2\text{temp.}) > \theta(\text{Pennes} - 2\text{temp.}) > \theta(\text{V} - \text{C} - 2\text{temp.}) \tag{40}$$

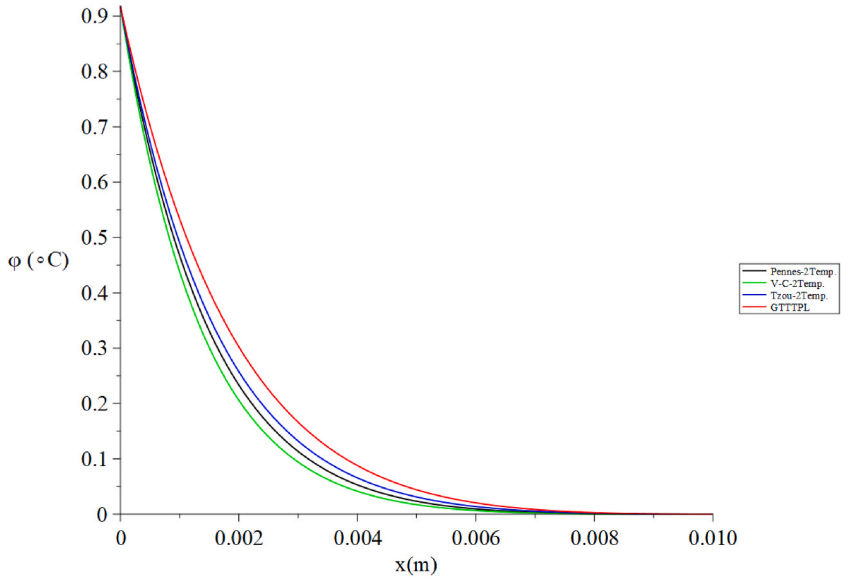

Fig. 10. The distributions of the conductive temperature increment distribution under different models when $\ell = 0.001$, $\beta \neq 0$, and $t(50\ \text{s}) < t_0(55\ \text{s})$.

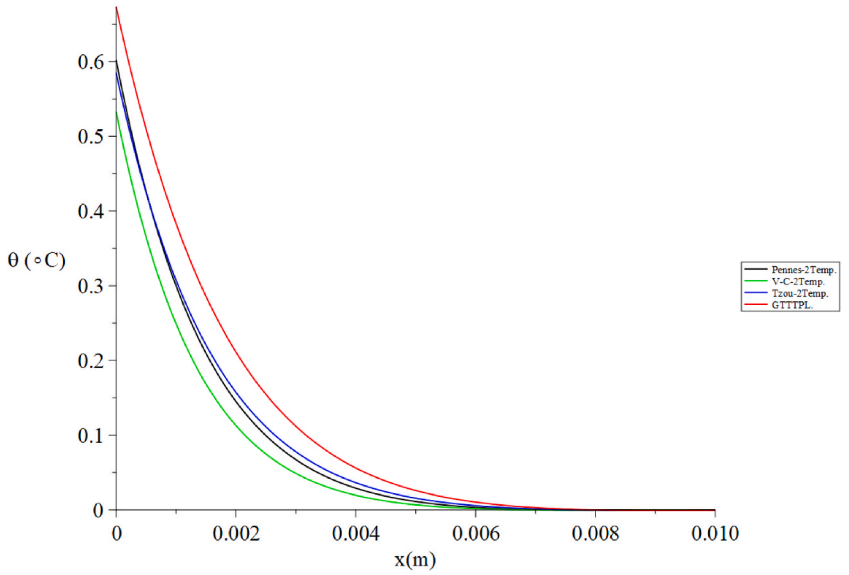

Fig. 11. The distributions of the dynamic temperature increment distribution under different models when $\ell = 0.001$, $\beta \neq 0$, and $t(50\ \text{s}) < t_0(55\ \text{s})$.

We can note that the dynamical temperature based on the four studied when the characteristic length $\ell = 0.001$ has the same beginning value when $x = 0$, while it has different values when $\ell = 0.003$ which confirms that the characteristic length has significant effects on the dynamical temperature increment distributions. In addition, decreasing the value of characteristic length makes the thermodynamic wave fall to zero quickly under the four studied models.

Figs. 6 and 7 illustrate the conductive temperature increment and dynamical temperature increment distributions, respectively, based on different models and different drift velocity values when $t = t_0 = 60(s)$ standing on the impact of the drift velocity on the thermal interaction on the skin tissue.

Fig. 6 illustrates that the effect of the drift velocity is major on the conductive temperature, where increasing its value leads to an increase in the conductive temperature increment. In addition, the values of conductive temperature increment based on the four studied models take the same order as in (39). Moreover, the speed of propagation of the thermo-conductive wave with zero drift velocity through the skin tissue falls to zero more quickly than with non-zero drift velocity under the four studied models.

Fig. 7 represents that the effect of the drift velocity is significant on the conductive temperature because increasing its value leads to

an increase in the dynamical temperature increment. In addition, the values of dynamical temperature increment based on the four studied models take the same order as in (40). We noted that the dynamical temperature is based on the four studied when the drift velocity $\beta = 0.0$ and $\beta \neq 0.0$ has different beginning values $x = 0$. Moreover, the speed of propagation of the thermodynamic wave with zero drift velocity through the skin tissue falls to zero more quickly than with non-zero drift velocity under the four studied models.

Figs. 8 and 9 illustrate the conductive temperature increment and dynamical temperature increment distributions, respectively, under the four studied models based on thermomass motion when $t > t_0$ and Figs. 10 and 11 illustrate the same distributions when $t < t_0$ studying the effect of the ramp-time heat parameter on the thermal interaction on the skin tissue.

Thus, we found that the ramp-time heat parameter has a major effect on the conductive and dynamical temperature increments based on thermomass motion, where increasing the value of the ramp-time heat parameter than the value of the time leads to a decrease in the values of the conductive and dynamical temperature increments. To explain, when the value of the relaxation time increases it means that the increasing of the thermal loading on the skin tissue up to the target value takes a longer time which generates a lower speed of propagation of the thermal waves. So, the ramp-time heat parameter may be used to adjust the rate at which the conductive and dynamic temperatures change inside the skin tissue.

4. Results validation

The current results for the models of Pennes, Vernotte-Cattaneo, and Tzou (DPL) give the same results as the same models in references [16–31], especially reference [26] which is closer to the current work.

5. Conclusions

The work aims to develop a new heat transfer model that considers thermomass motion and tests it on skin tissue. Four models were used: Pennes, Vernotte-Cattaneo, Tzou (DPL), and the general two-temperature three-phase-lag bioheat of Youssef. The equations controlling the general two-temperature three-phase-lag bioheat transmission model were solved directly in the Laplace transform domain. The study also explored ramp-type heat on the skin's surface and the temperature increase responses when ramp-time heat, characteristic length, and drift velocity parameters were changed. Thus, we have the following results:

1-The characterizing flow compressibility of the phonon gas parameter which is based on the drift velocity has significant impacts on the temperature increment based on all the studied bioheat conduction models.

2 Decreasing the value of characteristic length makes the thermoconductive and thermodynamic waves fall to zero more quickly under the four studied models. So the characteristic length could be used to control the propagation of the biothermal wave through the skin tissue.

3 The characteristic length parameter which is related to the drift velocity has major impacts on the conductive and dynamic temperature increment distributions in the context of all the studied bioheat conduction models.

4 Decreasing the value of drift velocity makes the thermoconductive and thermodynamic waves fall to zero more quickly under the four studied models. So, the drift velocity could be used to tune the propagation of the biothermal wave through the skin tissue.

5 The ramp-time heat parameter has significant influences on the thermal waves in all the examined heat conduction models and may be adjusted to control the propagation of the biothermal wave through the skin tissue.

6 Moreover, we can see that Youssef's (GTTTPL) model successfully explains the behaviour of skin tissue during heating.

CRediT authorship contribution statement

Eman A.N. Al-Lehaibi: Writing – review & editing, Writing – original draft, Visualization, Validation, Software. **Hamdy M. Youssef:** Methodology, Investigation, Formal analysis, Data curation, Conceptualization.

Declaration of competing interest

The authors declare that they have no known competing financial interests or personal relationships that could have appeared to influence the work reported in this paper.

References

[1] F. Xu, T. Lu, K. Seffen, E. Ng, Mathematical modeling of skin bioheat transfer, Appl. Mech. Rev. 62 (5) (2009) 050801.
[2] H.H. Pennes, Analysis of tissue and arterial blood temperatures in the resting human forearm, J. Appl. Physiol. 1 (2) (1948) 93–122.
[3] C. Cattaneo, A form of heat-conduction equations which eliminates the paradox of instantaneous propagation, Comptes Rendus 247 (1958) 431.
[4] P. Vernotte, Les paradoxes de la theorie continue de l'equation de la chaleur, Compt. Rendu 246 (1958) 3154–3155.
[5] F. Xu, K. Seffen, T. Lu, Non-Fourier analysis of skin biothermomechanics, Int. J. Heat Mass Tran. 51 (9–10) (2008) 2237–2259.
[6] C. Rossmann, D. Haemmerich, Review of temperature dependence of thermal properties, dielectric properties, and perfusion of biological tissues at hyperthermic and ablation temperatures, Crit. Rev. Biomed. Eng. 42 (6) (2014).
[7] D.Y. Tzou, A unified field approach for heat conduction from macro-to micro-scales, J. Heat Tran. 117 (1) (1995) 8–16.
[8] D. Jou, DY Tzou: macro-to microscale heat transfer. The lagging behaviour. Series in chemical and mechanical engineering, J. Non-Equilibrium Thermodyn. 23 (2) (1998) 192–193.

[9] M. Ozisik, D. Tzou, On the wave theory in heat conduction, J. Heat Tran. 116 (3) (1994) 526–535.
[10] H. Askarizadeh, H. Ahmadikia, Analytical analysis of the dual-phase-lag model of bioheat transfer equation during transient heating of skin tissue, Heat Mass Tran. 50 (12) (2014) 1673–1684.
[11] J. Dutta, B. Kundu, Exact analysis based on BDLTNE approach for thermal behaviour in living tissues during regional hyperthermia therapy, Acta Mech. 230 (8) (2019) 2853–2871.
[12] K.-C. Liu, Y.-N. Wang, Y.-S. Chen, Investigation on the bio-heat transfer with the dual-phase-lag effect, Int. J. Therm. Sci. 58 (2012) 29–35.
[13] K.-C. Liu, H.-T. Chen, Analysis for the dual-phase-lag bio-heat transfer during magnetic hyperthermia treatment, Int. J. Heat Mass Tran. 52 (5–6) (2009) 1185–1192.
[14] K.-C. Liu, H.-T. Chen, P.-J. Cheng, Inverse investigation of non-Fourier heat conduction in tissue, J. Therm. Biol. 62 (2016) 123–128.
[15] K.-C. Liu, H.-T. Chen, Investigation for the dual phase lag behavior of bio-heat transfer, Int. J. Therm. Sci. 49 (7) (2010) 1138–1146.
[16] Y. Zhang, Generalized dual-phase lag bioheat equations based on nonequilibrium heat transfer in living biological tissues, Int. J. Heat Mass Tran. 52 (21–22) (2009) 4829–4834.
[17] J. Dutta, B. Kundu, Thermal wave propagation in blood perfused tissues under hyperthermia treatment for unique oscillatory heat flux at skin surface and appropriate initial condition, Heat Mass Tran. 54 (11) (2018) 3199–3217.
[18] A. Moradi, H.Z. Poor, H. Moosavi, Analysis of the DPL Bio-Heat Transfer Equation with Constant and Time-dependent Heat Flux Conditions on Skin Surface, 2014.
[19] J. Liu, L.X. Xu, Estimation of blood perfusion using phase shift in temperature response to sinusoidal heating at the skin surface, IEEE (Inst. Electr. Electron. Eng.) Trans. Biomed. Eng. 46 (9) (1999) 1037–1043.
[20] H. Ahmadikia, R. Fazlali, A. Moradi, Analytical solution of the parabolic and hyperbolic heat transfer equations with constant and transient heat flux conditions on skin tissue, Int. Commun. Heat Mass Tran. 39 (1) (2012) 121–130.
[21] H.M. Youssef, N.A. Alghamdi, Modeling of one-dimensional thermoelastic dual-phase-lag skin tissue subjected to different types of thermal loading, Sci. Rep. 10 (1) (2020) 1–12.
[22] H.M. Youssef, A.A. El-Bary, Voltage and time required for irreversible thermal damage of tumor tissues during electrochemotherapy under Thomson effect, Mathematics 8 (9) (2020) 1488.
[23] H.M. Youssef, R.A. Salem, The dual-phase-lag bioheat transfer of a skin tissue subjected to thermo-electrical shock, Journal of Engineering and Thermal Sciences 2 (2) (2022) 114–123.
[24] H.-D. Wang, Theoretical and Experimental Studies on Non-fourier Heat Conduction Based on Thermomass Theory, Springer Science & Business Media, 2014.
[25] H.M. Youssef, A novel theory of generalized thermoelasticity based on thermomass motion and two-temperature heat conduction, J. Therm. Stresses 44 (2) (2021) 133–148.
[26] H.M. Youssef, E.A. Al-Lehaibi, General generalized thermoelasticity theory (GGTT), J. Therm. Anal. Calorim. (2023) 1–10.
[27] Z. Alqahtani, I. Abbas, A. El-Bary, A. Almuneef, Analytical solutions of thermomechanical interaction in living tissues under dual phase-lag model, Indian J. Phys. (2024) 1–7.
[28] I. Abbas, M. SaifAlDien, A.A. El-Bary, R.H. Egami, M. Elamin, Theoretical estimation of the thermal damages of living tissues caused by laser irradiation in tumor thermal therapy, Heliyon 10 (7) (2024) e29016.
[29] I. Abbas, A. Hobiny, A. El-Bary, Numerical solutions of nonlocal heat conduction technique in tumor thermal therapy, Acta Mech. 235 (4) (2024) 1865–1875.
[30] A. Hobiny, I. Abbas, Eigenvalue approach for investigating thermal and mechanical responses on living tissues during laser irradiation with experimental verification, Phys. Fluids 36 (3) (2024).
[31] I. Abbas, M.S. AlDien, M. Elamin, A. El-Bary, The effects of thermo-mechanical behavior of living tissues under thermal loading without energy dispassion, Coupled Systems Mechanics 13 (1) (2024) 61.
[32] T. Kumari, D. Kumar, K. Rai, S. Singh, Numerical solution of DPL heat transfer model in multi-layer biological skin tissue of the living body during hyperthermia treatment, Mech. Base. Des. Struct. Mach. 51 (1) (2023) 159–178.
[33] H.H. Sherief, M.F. Zaky, M.F. Abbas, S.A. Mahrous, Mathematical modeling of heat transfer in tissues with skin tumor during thermotherapy, PLoS One 19 (5) (2024) e0298256.
[34] H.-J. Jiang, Q.-Z. Guo, X.-G. Wang, N.-H. Gao, Analytical solution of three-dimensional temperature field for skin tissue considering blood perfusion rates under laser irradiation and thermal damage analysis, Optik 312 (2024) 171982.
[35] P. Wongchadakul, P. Rattanadecho, T. Wessapan, Implementation of a thermomechanical model to simulate laser heating in shrinkage tissue (effects of wavelength, laser irradiation intensity, and irradiation beam area), Int. J. Therm. Sci. 134 (2018) 321–336.
[36] H.M. Youssef, N. Alghamdi, Characterization of thermal damage due to two-temperature high-order thermal lagging in a three-dimensional biological tissue subjected to a rectangular laser pulse, Polymers 12 (4) (2020) 922.
[37] H.M. Youssef, N.A. Alghamdi, Three-dimensional biological tissue under high-order effect of two-temperature thermal lagging to thermal responses due to a laser irradiation, Vibroengineering PROCEDIA 22 (2019) 112–117.
[38] D. Tzou, M.-t.M.H. Transfer, The Lagging Behavior, Taylor Francis, Washington, 1997.
[39] F. Xu, T. Lu, K. Seffen, Biothermomechanical behavior of skin tissue, Acta Mech. Sin. 24 (1) (2008) 1–23.